

# On the surface tension of neutron star matter

Jorge A. Rueda<sup>a,b</sup>, Remo Ruffini<sup>a,b,c</sup>, Yuan-Bin Wu<sup>a,b,c,\*</sup>, She-Sheng Xue<sup>a,b</sup>

<sup>a</sup>*Dipartimento di Fisica and ICRA, Sapienza Università di Roma,  
P.le Aldo Moro 5, I-00185 Rome, Italy*

<sup>b</sup>*ICRANet, P.zza della Repubblica 10, I-65122 Pescara, Italy*

<sup>c</sup>*ICRANet, University of Nice-Sophia Antipolis, 28 Av. de Valrose,  
06103 Nice Cedex 2, France*

---

## Abstract

It has been recently shown that taking into account strong, weak, electromagnetic, and gravitational interactions, and fulfilling the global charge neutrality of the system, a transition layer will happen between the core and crust of neutron stars, at the nuclear saturation density. We use relativistic mean field theory together with the Thomas-Fermi approximation to study the detailed structure of this transition layer and calculate its surface and Coulomb energy. We find that the surface tension is proportional to a power-law function of the baryon number density in the core bulk region. We also analyze the influence of the gravitational field and the electron component on the structure of the transition layer and the value of the surface tension to compare and contrast with known phenomenological results in nuclear physics. Based on the above results we study the instability against Bohr-Wheeler surface deformations in the case of neutron stars obeying global charge neutrality. Assuming the core-crust transition at nuclear density  $\rho_{core} \approx 2.7 \times 10^{14} \text{ g cm}^{-3}$ , we find that the instability sets the upper limit to the crust density,  $\rho_{crust}^{crit} \approx 1.2 \times 10^{14} \text{ g cm}^{-3}$ . This result implies a non-zero lower limit to the maximum electric field of the core-crust transition surface and makes inaccessible a limit of quasi-local charge neutrality reachable in the limit  $\rho_{crust} = \rho_{core}$ . The general framework presented here can be also applied to study the stability of sharp phase-transitions in hybrid stars as well as in strange stars both bare and with outer crust. The results of this work open the way to a more general analysis of the stability of these transition surfaces accounting for other effects such as gravitational binding, centrifugal repulsion, magnetic field induced by rotating electric field and therefore magnetic dipole-dipole interactions.

**Keywords:** Surface tension, Nuclear matter, Neutron stars, General relativity

---

---

\*Corresponding author

Email addresses: [jorge.rueda@icra.it](mailto:jorge.rueda@icra.it) (Jorge A. Rueda), [ruffini@icra.it](mailto:ruffini@icra.it) (Remo Ruffini), [wuyb@icranet.org](mailto:wuyb@icranet.org) (Yuan-Bin Wu), [xue@icra.it](mailto:xue@icra.it) (She-Sheng Xue)

## 1. Introduction

The relativistic mean field theory (RMFT) of nuclear matter and Thomas-Fermi model have attracted great attention during the last few decades. The simplest relativistic model of nuclear matter that accounts for the saturation properties of symmetric nuclear matter includes one scalar field which gives the attractive long-range part of the nuclear force and one vector field which gives the repulsive short-range; these two meson fields interact with nucleons through Yukawa couplings. This so-called  $\sigma$ - $\omega$  model has been considered by Duerr [1], Miller and Green [2], and later by Walecka [3]. The relevance of such interactions and relativistic effects in the determination of the equation of state and in the properties of nuclear matter such as compressibility and the nucleon effective mass was clearly pointed out in Refs. [2, 4, 5]. In Refs. [6, 7, 8], Lee and collaborators considered a model with only one scalar field with self-interaction up to quartic order based on the  $\sigma$ -model. They introduced the repulsive contribution of nuclear force through a *hard-sphere* model that artificially increases the nucleon Fermi momentum, emulating the effect of a massive vector field coupled to nucleons. The importance of allowing scalar meson self-interactions (cubic and quartic terms in the scalar field potential) as adjustable parameters to reproduce physical nuclear properties and not due to renormalization (see e.g. [3]) was stressed in Refs. [5, 9, 10, 11]. As recognized in Ref. [5], it is necessary to introduce additional isovector fields to obtain the agreement with the empirical symmetry energy of nuclear matter at the saturation density. The model contained Dirac nucleons together with a self-interacting scalar  $\sigma$  and a vector meson  $\omega$  as well as an isovector meson  $\rho$  has been widely used to the end.

With a very limited number of parameters, the RMFT has been shown to be able to give a quantitative description of a variety of nuclear properties [12, 13, 14]. Recently, taking into account the electromagnetic and weak interactions, the RMFT with the Thomas-Fermi approximation has gained remarkable successes in understanding the inhomogeneous structures and properties of low-density nuclear matter which is realized in the supernovae core or in the crust of neutron stars (see e.g. Refs. [15, 16, 17, 18]). The surface properties of nuclear matter such as surface tension and curvature energy play an important role in the description of these structures and also in other phenomena, for instance saddle-point configurations in nuclear fission, fragment distributions in heavy-ion collisions, and phase transition between different phases of nuclear matter.

The nuclear surface properties at saturation density have been analyzed for a long time in the semi-infinite nuclear matter model using RMFT [3] or effective field theory [19, 20, 21] with the Thomas-Fermi approximation or Hartree-Fock approximation [5, 22, 23, 24, 25, 26, 27, 28, 29, 30]. In the supranuclear regime realized in the interior of neutron stars, there is the possibility that phase transition occurs from hadronic to pion and kaon condensed phase as well as to quark matter phase (see e.g. [31, 32, 33]). The surface tension of the transition layer between the hadronic and kaon condensed or quark matter phases has

been calculated in the semi-infinite matter model and the surface tension plays an important role for the structure of the phase transition region [34, 35]. In the low-density (density smaller than the saturation density) case, as pointed out in [36], the shape of constituent nuclei is expected to change from spherical droplet to the so-called nuclear pasta structures such as cylindrical rod, slab, cylindrical tube, and spherical bubble. The surface tensions of nuclear pasta structures have been investigated and it has pointed out that the pasta phase strongly depends on the value of the surface tension [15, 16, 18].

The importance of the extension of the Thomas-Fermi approximation to general relativistic systems such as neutron stars was emphasized in Ref. [37]. We showed there that the traditionally imposed condition of local charge neutrality is not consistent with the field equations and microphysical equilibrium for a system of neutrons, protons, and electrons in  $\beta$ -equilibrium and obeying relativistic quantum statistics. Thus, only the condition of global but not local charge neutrality can be imposed. This leads to the appearance of gravito-polarization in the cores of neutron stars. The generalization of such a work to the case where the strong interactions between nucleons are accounted for was presented in [38]. Both the Thomas-Fermi approximation and RMFT were used. It was shown that the Einstein-Maxwell-Thomas-Fermi system of equations within RMFT supersede the traditional Tolman-Oppenheimer-Volkoff (TOV) [39, 40] equations used for the construction of neutron star configurations.

Realistic neutron star configurations including all the interactions between particles and the presence of a crust below nuclear density, were constructed in Ref. [41] by solving numerically the Einstein-Maxwell-Thomas-Fermi equations fulfilling the condition of global charge neutrality. As pointed out in [41], the self-consistent solution of these new equations of equilibrium leads to the existence of a transition layer between the core and the crust of the star. This is markedly different from the neutron star structure obtained from the solution of the TOV equations imposing local charge neutrality [42], leading to a new mass-radius relation of neutron stars. Such core-crust transition layer occurs near the nuclear saturation density. The core (bulk region) inside this transition layer is a hadronic phase and the crust outside this transition is composed by the nuclei lattice and the ocean of relativistic degenerate electrons and possibly neutrons at densities below nuclear saturation and larger than the estimated neutron drip value  $\sim 4.3 \times 10^{11} \text{ g cm}^{-3}$ . Inside the transition region it is developed a very strong electric field overwhelming the critical value for vacuum break-down  $E_c = m_e^2 c^3 / (e\hbar)$ , where  $m_e$  is the electron rest-mass. The  $e^+e^-$  pair creation out from vacuum is however forbidden in the system due to the Pauli blocking of degenerate electrons.

In this article we study the detailed structure of this transition layer formed near the nuclear saturation density. We calculate all the contributions to the surface tension as well as the electrostatic energy stored in this core-crust layer. We analyze the stability of these systems under the Bohr-Wheeler fission mechanism [43]. We analyze the role of the electron contribution and compare and contrast the surface energy of these neutron stars with the phenomenological results in nuclear physics for both ordinary and superheavy nuclei.

The article is organized as follows. In Sec. 2, we study the surface structure and the surface tension as well as the Coulomb energy for neutron star matter without the influence of the gravitational field. We formulate in Sec. 2.1 the relativistic equations for a system of neutrons, protons and electrons fulfilling strong and electromagnetic interactions as well as  $\beta$ -equilibrium. In Sec. 2.2, we use the semi-infinite matter model [44] to formulate the equations governing the surface tension for the transition layer of this system when the electron density is nearly equal to the proton density in the core bulk region. In Sec. 2.3, we calculate the surface structure and solve these equations to obtain the surface tension and the Coulomb energy at the nuclear saturation density and neglecting the presence of the crust. Then we study in Sec. 2.4 the dependence of the surface tension and the Coulomb energy on the baryon number density. In Sec. 2.5, we study the influence of fermion densities in the outside region (crust) on the surface tension and the Coulomb energy. In Sec. 3, we study the structure and the surface tension as well as the Coulomb energy for the core-crust transition region in the presence of the gravitational field within the framework of general relativity. We present the set of general relativistic equations in Sec. 3.1. Then in Sec. 3.2, we calculate the surface tension for the transition layer with these equations including the presence of the gravitational interactions. In Sec. 4, we calculate the surface tension and the Coulomb energy for the transition layer of the system when the electron density is smaller than the proton density in the bulk region and compare the results with known phenomenological results in nuclear physics. We finally summarize and conclude in Sec. 5. We use units with  $\hbar = c = 1$  throughout the article.

## 2. Surface properties for neutron star matter without gravitational interaction

### 2.1. Relativistic equations of motion

As described in Ref. [41], the system we consider is composed of degenerate neutrons, protons, and electrons fulfilling global charge neutrality and  $\beta$ -equilibrium. To describe the nuclear interactions, here we employ the RMFT with the Thomas-Fermi approximation. We adopt the phenomenological nuclear model of Boguta and Bodmer [5].

Taking into account the strong, electromagnetic, and weak interactions, the total Lagrangian density of the system is given by

$$\mathcal{L} = \mathcal{L}_f + \mathcal{L}_\sigma + \mathcal{L}_\omega + \mathcal{L}_\rho + \mathcal{L}_\gamma + \mathcal{L}_{int}, \quad (1)$$

where the Lagrangian densities for the free-fields are

$$\mathcal{L}_\gamma = -\frac{1}{16\pi}F_{\mu\nu}F^{\mu\nu}, \quad (2)$$

$$\mathcal{L}_\sigma = \frac{1}{2}\nabla_\mu\sigma\nabla^\mu\sigma - U(\sigma), \quad (3)$$

$$\mathcal{L}_\omega = -\frac{1}{4}\Omega_{\mu\nu}\Omega^{\mu\nu} + \frac{1}{2}m_\omega^2\omega_\mu\omega^\mu, \quad (4)$$

$$\mathcal{L}_\rho = -\frac{1}{4}\mathcal{R}_{\mu\nu}\mathcal{R}^{\mu\nu} + \frac{1}{2}m_\rho^2\rho_\mu\rho^\mu, \quad (5)$$

where  $\Omega_{\mu\nu} \equiv \partial_\mu\omega_\nu - \partial_\nu\omega_\mu$ ,  $\mathcal{R}_{\mu\nu} \equiv \partial_\mu\rho_\nu - \partial_\nu\rho_\mu$ ,  $F_{\mu\nu} \equiv \partial_\mu A_\nu - \partial_\nu A_\mu$  are the field strength tensors for the vector meson field  $\omega$ , isovector meson field  $\rho$ , and electromagnetic field  $A$  respectively,  $\nabla_\mu$  stands for covariant derivative. The Lorenz gauge is adopted for the fields  $A_\mu$ ,  $\omega_\mu$ , and  $\rho_\mu$ .

The Lagrangian density for the three fermion species is

$$\mathcal{L}_f = \sum_{i=e,N} \bar{\psi}_i(i\gamma^\mu\partial_\mu - m_i)\psi_i, \quad (6)$$

where  $\psi_N$  is the nucleon isospin doublet,  $\psi_e$  is the electronic singlet, and  $m_i$  stands for the rest-mass of each  $i$ -fermion specie.

The scalar self-interaction potential is

$$U(\sigma) = \frac{1}{2}m_\sigma^2\sigma^2 + \frac{1}{3}g_2\sigma^3 + \frac{1}{4}g_3\sigma^4. \quad (7)$$

The interacting part of the Lagrangian density is given by

$$\mathcal{L}_{int} = -g_\sigma\sigma\bar{\psi}_N\psi_N - g_\omega\omega_\mu J_\omega^\mu - g_\rho\rho_\mu J_\rho^\mu + eA_\mu J_{\gamma,e}^\mu - eA_\mu J_{\gamma,N}^\mu, \quad (8)$$

where the conserved currents are

$$J_\omega^\mu = \bar{\psi}_N\gamma^\mu\psi_N, \quad (9)$$

$$J_\rho^\mu = \bar{\psi}_N\tau_3\gamma^\mu\psi_N, \quad (10)$$

$$J_{\gamma,e}^\mu = \bar{\psi}_e\gamma^\mu\psi_e, \quad (11)$$

$$J_{\gamma,N}^\mu = \bar{\psi}_N\left(\frac{1+\tau_3}{2}\right)\gamma^\mu\psi_N, \quad (12)$$

with  $g_\sigma$ ,  $g_\omega$ , and  $g_\rho$  the coupling constants of the  $\sigma$ ,  $\omega$  and  $\rho$  fields, and  $e$  is the fundamental electric charge.  $\tau_3$  is the third component of the isospin Pauli matrices.

Within the Thomas-Fermi approximation, the position-dependent equations

of motion for this system are given by

$$\nabla^2 V = -4\pi e(n_p - n_e), \quad (13)$$

$$\nabla^2 \sigma = \partial_\sigma U(\sigma) + g_s n_s, \quad (14)$$

$$\nabla^2 \omega = -(g_\omega J_0^\omega - m_\omega^2 \omega), \quad (15)$$

$$\nabla^2 \rho = -(g_\rho J_0^\rho - m_\rho^2 \rho), \quad (16)$$

$$E_e^F = \mu_e - eV = \text{constant}, \quad (17)$$

$$E_p^F = \mu_p + g_\omega \omega + g_\rho \rho + eV = \text{constant}, \quad (18)$$

$$E_n^F = \mu_n + g_\omega \omega - g_\rho \rho = \text{constant}, \quad (19)$$

where the notation  $\omega_0 \equiv \omega$ ,  $\rho_0 \equiv \rho$ , and  $A_0 \equiv V$  for the time components of the meson fields have been introduced. Here  $\mu_i = \sqrt{(P_i^F)^2 + \tilde{m}_i^2}$  and  $n_i = (P_i^F)^3 / (3\pi^2)$  are the free chemical potential and number density of the  $i$ -specie with Fermi momentum  $P_i^F$ . The particle effective masses are  $\tilde{m}_N = m_N + g_s \sigma$  and  $\tilde{m}_e = m_e$ .

The generalized chemical potential of electrons, protons, and neutrons,  $E_e^F$ ,  $E_p^F$ , and  $E_n^F$ , derived from the thermodynamic equilibrium conditions given by the statistical physics of multicomponent systems, are linked by the  $\beta$ -equilibrium [45] of protons, neutrons, and electrons

$$E_n^F = E_p^F + E_e^F. \quad (20)$$

The scalar density  $n_s$  is given by the expectation value

$$n_s = \langle \bar{\psi}_N \psi_N \rangle = \frac{2}{(2\pi)^3} \sum_{i=n,p} \int_0^{P_i^F} d^3 k \frac{\tilde{m}_N}{\epsilon_i(k)}, \quad (21)$$

where  $\epsilon_i(k) = \sqrt{k^2 + \tilde{m}_i^2}$  is the single particle energy. In the static case, only the time components of the covariant currents survive, i.e.  $\langle \bar{\psi}(x) \gamma^i \psi(x) \rangle = 0$ . The nonvanishing components of the currents are

$$J_0^{ch} = n_p - n_e, \quad (22)$$

$$J_0^\omega = n_b = n_n + n_p, \quad (23)$$

$$J_0^\rho = n_p - n_n, \quad (24)$$

here  $n_b = n_p + n_n$  is the baryon number density.

For the system of static uniform matter in its ground state, the source currents  $\bar{\psi}\psi$  and  $\bar{\psi}\gamma^\mu\psi$  are position-independent. The derivative terms in Eqs. (14)-(16) are zero. As a consequence, equations (14)-(16) reduce to the simpler form

$$\partial_\sigma U(\sigma) + g_s n_s = 0, \quad (25)$$

$$-(g_\omega J_0^\omega - m_\omega^2 \omega) = 0, \quad (26)$$

$$-(g_\rho J_0^\rho - m_\rho^2 \rho) = 0. \quad (27)$$

## 2.2. Surface tension for semi-infinite matter

As shown in [41], in the bulk hadronic phase of neutron star cores, the charge separation is very small, so the electron density  $n_{eb}$  is nearly equal to the proton density  $n_{pb}$ . For the system with  $n_{eb} \simeq n_{pb}$  in the bulk region and obeying global charge neutrality, we can apply the semi-infinite matter model to calculate the surface tension. We construct the surface tension for the transition layer of this system following the method of Baym, Bethe, and Pethick (BBP) [44].

In the semi-infinite matter model, one assumes a plane surface (with small thickness compared with the bulk region size) perpendicular to the  $z$ -axis separating two semi-infinite regions, represented here by the inside core bulk and the outside crust. The number density of the  $i$ -specie ( $i = n, p, e$ ) fermion  $n_i(\vec{r})$  approaches the bulk density of the  $i$ -specie fermion  $n_{ib}$  as the position  $z \rightarrow -\infty$ , and approaches the density in the outside region of the  $i$ -specie fermion  $n_{io}$  as the  $z \rightarrow +\infty$ . The semi-infinite matter is a one-dimensional system, namely there is only  $z$ -dependence. To construct the surface tension, one imagines a reference system with a sharp surface at  $z = a_i$  at which fermion densities and meson fields fall discontinuously from the bulk region to the outside region. Following Ref. [44], the location of the reference surface for the  $i$ -specie fermion is defined by the condition that the reference system has the same number of the  $i$ -specie fermion as the original system

$$\int_{z=-\infty}^{a_i} d^3r [n_i(\vec{r}) - n_{ib}] + \int_{z=a_i}^{\infty} d^3r [n_i(\vec{r}) - n_{io}] = 0; \quad i = n, p, e. \quad (28)$$

Apply the definition of reference surface in Eq. (28) to neutron, proton, and electron yields slightly different reference surface.

Similar to the definition of reference surface for fermion, we define the location of the reference surfaces for meson fields by

$$\int_{z=-\infty}^{a_i} d^3r [F_i(\vec{r}) - F_{ib}] + \int_{z=a_i}^{\infty} d^3r [F_i(\vec{r}) - F_{io}] = 0; \quad i = \sigma, \omega, \rho, \quad (29)$$

where  $F_i(\vec{r})$  is the time component of the  $i$ -specie meson field,  $F_{ib}$  is the time component of the  $i$ -specie meson field in the bulk region, and  $F_{io}$  is the time component of the  $i$ -specie meson field in the outside region.

Thus, the total surface tension can be written as the sum of three contributions

$$\sigma_t = \sigma_N + \sigma_e + \sigma_C, \quad (30)$$

where we have introduced the nuclear surface tension following the method of BBP [44],

$$\sigma_N = \sum_{i=n,p,\sigma,\omega,\rho} \left\{ \int_{-\infty}^{a_i} [\epsilon_i(z) - \epsilon_{ib}] dz + \int_{a_i}^{\infty} [\epsilon_i(z) - \epsilon_{io}] dz \right\}, \quad (31)$$

the electron surface tension

$$\sigma_e = \left\{ \int_{-\infty}^{a_e} [\epsilon_e(z) - \epsilon_{eb}] dz + \int_{a_e}^{\infty} [\epsilon_e(z) - \epsilon_{eo}] dz \right\}, \quad (32)$$

and the surface tension for the electric field as

$$\sigma_C = \int_{-\infty}^{\infty} \epsilon_E(z) dz, \quad (33)$$

with  $\epsilon_i(z)$  the energy density of the  $i$ -specie fermion or meson field,  $\epsilon_{ib}$  is the energy density of the  $i$ -specie fermion or meson field in the bulk region,  $\epsilon_{io}$  is the energy density of the  $i$ -specie fermion or meson field in the outside region, and  $\epsilon_E(z) = E^2/(8\pi)$  is the electrostatic energy density.

It is important to remark here that owing to the small charge separation present in the system in the core bulk region, we can assume that the electric field only exists in the transition layer surface. Thus we can consider the electrostatic energy as a surface property of the system, hence contributing to the surface energy. This is a major difference between the present system and an ordinary nucleus where the electrostatic energy is a volume property.

The relation between the surface energy and Coulomb energy is very important for a nucleus. As shown by Bohr and Wheeler [43] when the condition

$$E_{coul} > 2E_{sur} \quad (34)$$

satisfies, the nucleus becomes unstable against nuclear fission, here  $E_{coul}$  is the Coulomb energy of the nucleus and  $E_{sur}$  is the surface energy of the nucleus. It is important to recall that the idealized picture of the deformed nucleus of Bohr and Wheeler is represented by two positively charged spheres joined by a nuclear attraction neck. It is thus the interplay of the Coulomb and nuclear surface energies that determines the lower energy state. Following this argument one could think that since we are treating here a globally neutral system such an instability mechanism is absent. However, the condition (34) can be also obtained by requesting that a uniformly charged spheroid constructed from an axially symmetric deformation at constant volume of a uniformly charged sphere, be energetically favorable. From a careful look at the derivation of Eq. (34), see e.g. Ref.[46], it can be seen that this result follows from the fact that Coulomb energy of the unperturbed system (the sphere) depends on the radius as  $E_{coul} \propto R^{-1}$ . Such an inverse radius dependence holds also in the case of a uniformly charged shell, and also in the case of the globally neutral massive nuclear density cores studied in Refs. [47, 48]; which fully reflect the properties of the system studied in this work. We then expect that the Bohr-Wheeler condition of instability against fission given by Eq. (34) applies also to our system. Clearly such a condition is obtained keeping the system at nuclear density and neglecting the the extra binding effect of gravity.

In thermodynamics, the surface tension is related to the mechanical work needed to increase a surface area [49],

$$dW = \sigma dS, \quad (35)$$

here  $\sigma$  is the surface tension,  $dS$  is the variation of the surface area, and  $dW$  is the mechanical work needed to increase the surface area of the system. In this



point of view, a system with a positive surface tension has an attractive nature, and a system with a negative surface tension has a repulsive nature.

The Eqs. (30)–(33) show that the surface tension mainly depends on the fermion density and meson field profiles and the energy densities of fermions and meson fields. For semi-infinite matter, the system is only  $z$ -dependence and Eqs. (13)–(16) become

$$\frac{d^2 V}{dz^2} = -4\pi e(n_p - n_e), \quad (36)$$

$$\frac{d^2 \sigma}{dz^2} = \partial_\sigma U(\sigma) + g_s n_s, \quad (37)$$

$$\frac{d^2 \omega}{dz^2} = -(g_\omega J_0^\omega - m_\omega^2 \omega), \quad (38)$$

$$\frac{d^2 \rho}{dz^2} = -(g_\rho J_0^\rho - m_\rho^2 \rho). \quad (39)$$

The energy density of the  $i$ -specie fermion is given by

$$\begin{aligned} \epsilon_i(z) = & \frac{1}{8\pi^2} \left\{ P_i^F \sqrt{(P_i^F)^2 + \tilde{m}_i^2} [2(P_i^F)^2 + \tilde{m}_i^2] \right. \\ & \left. - \tilde{m}_i^4 \ln \frac{P_i^F + \sqrt{(P_i^F)^2 + \tilde{m}_i^2}}{\tilde{m}_i} \right\}, \end{aligned} \quad (40)$$

and the energy densities of the meson fields are

$$\epsilon_\sigma(z) = \frac{1}{2} \left( \frac{d\sigma}{dz} \right)^2 + U(\sigma), \quad (41)$$

$$\epsilon_\omega(z) = \frac{1}{2} \left( \frac{d\omega}{dz} \right)^2 + \frac{1}{2} m_\omega^2 \omega^2, \quad (42)$$

$$\epsilon_\rho(z) = \frac{1}{2} \left( \frac{d\rho}{dz} \right)^2 + \frac{1}{2} m_\rho^2 \rho^2, \quad (43)$$

$$\epsilon_E(z) = \frac{1}{8\pi} \left( \frac{dV}{dz} \right)^2. \quad (44)$$

We can solve Eqs. (36)–(39) and Eqs. (17)–(19) to obtain the fermion density and meson field profiles. This system of equations can be numerically solved with appropriate boundary conditions.

The parameters of the nuclear model, namely the coupling constants  $g_\sigma$ ,  $g_\omega$ , and  $g_\rho$ , the meson masses  $m_\sigma$ ,  $m_\omega$ , and  $m_\rho$ , and the third and fourth order constants of the self-scalar interaction  $g_2$  and  $g_3$  are fixed by fitting experimental properties of nuclei, such as saturation density, binding energy per nucleon, symmetry energy, surface energy, and nuclear incompressibility. We here use the parameters of the NL3 parameterization [50], shown in Table 1.

	NL3		NL3
$m_\sigma$ (MeV)	508.194	$g_\omega$	12.8680
$m_\omega$ (MeV)	782.501	$g_\rho$	4.4740
$m_\rho$ (MeV)	763.000	$g_2$ (fm <sup>-1</sup> )	-10.4310
$g_\sigma$	10.2170	$g_3$	-28.8850

Table 1: The parameters of the nuclear model from NL3.

### 2.3. Surface structure and surface tension at the nuclear saturation density

The boundary conditions for the numerical integration are fixed through the following procedure. We start assuming that the bulk region is formed by uniform matter, so we can apply Eqs. (25)–(27) to the bulk core. We assume the baryon number density of the bulk region to be the nuclear saturation density,  $n_{bb} = n_{nb} + n_{pb} = n_{nucl} = 0.16 \text{ fm}^{-3}$ .

First we will compute the surface properties in the case when the fermion densities and meson fields to be zero in the outside region, namely neglecting the influence of the outside crust region. We have also in the bulk core the condition  $n_{pb} \simeq n_{eb}$ . Taking into account the above conditions, we can solve the equations (25)–(27) together with the  $\beta$ -equilibrium (20) in the bulk region to obtain  $\sigma_b$ ,  $\omega_b$ ,  $\rho_b$ ,  $n_{nb}$ ,  $n_{pb}$ , and  $n_{eb}$ . Using this bulk region values as boundary conditions, we solve Eqs. (36)–(39) and Eqs. (17)–(19) in the surface region. The results are shown in Fig. 1. Since the fermion densities tend to be zero in the outside region, the thickness of the surface region for electrons should be infinite. However we just show the results up to a very small electron density here, due to the plot-scale and the accuracy of the numerical calculation.

There exist two scale lengths in this system, one is related to the nuclear interactions ( $\sim \lambda_\pi = \hbar/(m_\pi c) \sim 1.5 \text{ fm}$ ) and another one is related to the electron screening ( $\sim \lambda_e = \hbar/(m_e c) \sim 100 \text{ fm}$ ). It is shown in Fig. 1 that the transition layer can be divided by three regions due to the existence of these two different scale lengths. (I) due to the electromagnetic interaction, all the fields vary slowly with the length scale  $\sim \lambda_e$ . In this region the effect of the Coulomb interaction is clear: on the proton density profile we can see a bump due to Coulomb repulsion while the electron density profile decreases. The neutrons also feels this Coulomb effect indirectly due to the coupled nature of the system of equations. But this effect is much smaller than the effect on protons and it is not appreciable in Fig. 1 due to the plot-scale. (II) due to the nuclear interactions, a sharp decrease of the proton and neutron densities happens in the length scale  $\lambda_\pi$ . It can be seen a neutron skin effect, which makes the scale of the neutron density falloff slightly larger with respect to the proton one, in analogy to the one observed in heavy nuclei and in neutron rich nuclei [51]. (III) the electron density decreases smoothly in the length scale  $\lambda_e$  and this produces the total screening of the positively charged core. As shown in Fig. 1, we can obtain an electric field that is larger than critical field in the surface region. However, no  $e^+e^-$  pair can be produced in this region due to the Pauli blocking

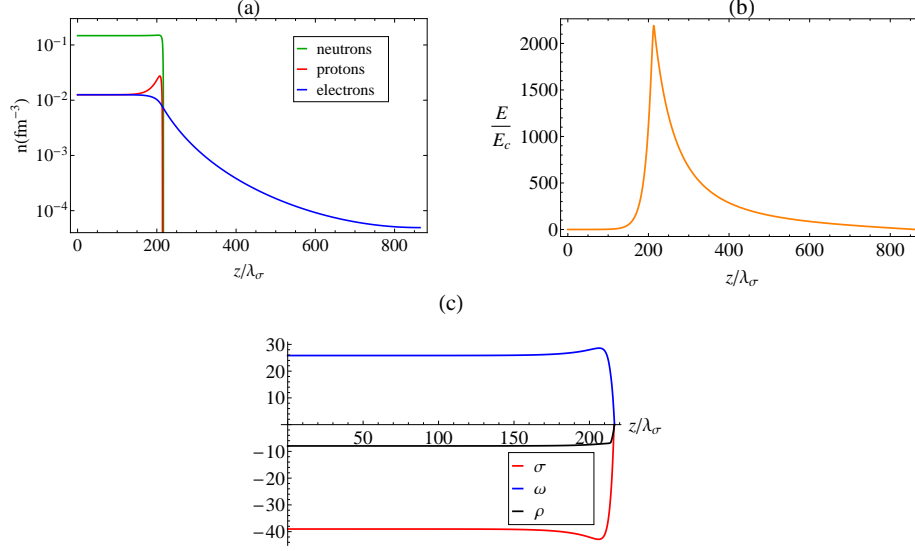


Figure 1: (a): fermion density profiles in units of  $\text{fm}^{-3}$ . (b): electric field in units of the critical field  $E_c = m_e^2 c^3 / (e\hbar)$ . (c): meson fields  $\sigma$ ,  $\omega$ , and  $\rho$  in the unit of MeV. Here the baryon number density of the bulk region is the nuclear saturation value, and the fermion densities and meson fields tend to be zero in the outside region.  $\lambda_\sigma = \hbar / (m_\sigma c) \sim 0.4$  fm is the Compton wavelength of the  $\sigma$  meson.

owing to the presence of degenerate electrons.

In order to study the effect of the  $\rho$  meson, we solve Eqs. (36)–(39) and Eqs. (17)–(19) without the presence of the  $\rho$  meson. The results are shown in Fig. 2. The fermion density and meson field profiles are similar to those in the case with the presence of the  $\rho$  meson, as shown in Figs. 1 and 2. Due to the absence of the  $\rho$  meson, the proton (and hence the electron) to neutron density ratio decreases, so if the baryon density is the same it causes a lowering of the electric field intensity.

	$\sigma_t$	$\sigma_N$	$\sigma_e$	$\sigma_C$
$\sigma \ \omega$	6.28	7.07	-1.72	0.92
$\sigma \ \omega \ \rho$	3.10	7.30	-8.34	4.14

Table 2: Total and specific surface tensions in  $\text{MeV fm}^{-2}$  of semi-infinite matter with and without the presence of the  $\rho$  meson. Here the baryon number density in the bulk region is set to the nuclear saturation value and the fermion densities and meson fields tend to be zero in the outside region.

Using the definitions in Eqs. (30)–(33), we can calculate the surface tensions for this transition layer. The results are shown in Table 2. The presence of  $\rho$  decreases the total surface tension  $\sigma_t$  but increases the Coulomb energy, and so  $\sigma_C$ . We can see that the difference of the surface tension for nucleons  $\sigma_N$

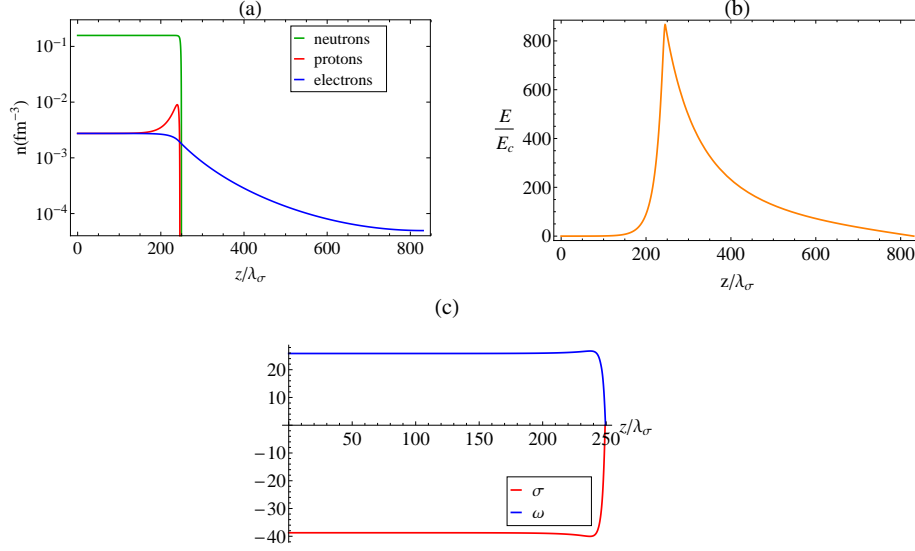


Figure 2: (a): fermion density profiles in units of  $\text{fm}^{-3}$ . (b): electric field in units of the critical field  $E_c$ . (c): meson fields  $\sigma$  and  $\omega$  in the unit of MeV. Here the baryon number density of the bulk region is the nuclear saturation density, the fermion densities and meson fields tend to be zero in the outside region, and  $\rho$  meson is not included in the calculation.

in the presence and absence of the  $\rho$  meson is relatively small with respect to the changes on the electron component and the electric field. We can explain this small difference from the fact that although the  $\rho$  meson increases the proton to neutron density ratio, in neutron stars the  $\beta$ -equilibrium in presence of degenerate electrons leads to a high isospin asymmetry  $1 - 2Z/A \approx 1$ , hence the system is still dominated by the neutron component, as we show below.

It is interesting to compare the above results with the ones in Ref. [35] where the surface tension of the interface between quark matter in color-flavor-locked (CFL) phase and ordinary hadronic phase. The surface tension was obtained as the sum of two contributions: (I) the first due to the QCD-scale interface, which they treated as infinitely sharp and estimated based on dimensional analysis,  $\sigma_{QCD} \sim 300 \text{ MeV fm}^{-2}$ ; (II) a surface tension  $\sigma_{boundarylayer} \approx 420 \text{ MeV fm}^{-2}$  associated to the electron screening length and computed from the particle number density profiles similarly as here. Thus, they obtained a total surface tension  $\sigma_{sur} = \sigma_{QCD} + \sigma_{boundarylayer} \approx 720 \text{ MeV fm}^{-2}$ . The difference between our result in Table 2 and the result in Ref. [35] is mainly due to the fact that the CFL-hadronic interface occurs in the inner core of the neutron star at baryon densities much higher than the nuclear saturation value separating the core and the crust.

In order to understand where the surface tension comes from, we calculate

the contribution of each fermion and meson field to the surface tension as

$$\sigma_n = \int_{-\infty}^{a_n} [\epsilon_n(z) - \epsilon_{nb}] dz + \int_{a_n}^{\infty} [\epsilon_n(z) - \epsilon_{no}] dz, \quad (45)$$

$$\sigma_p = \int_{-\infty}^{a_p} [\epsilon_p(z) - \epsilon_{pb}] dz + \int_{a_p}^{\infty} [\epsilon_p(z) - \epsilon_{po}] dz, \quad (46)$$

$$\sigma_e = \int_{-\infty}^{a_e} [\epsilon_e(z) - \epsilon_{eb}] dz + \int_{a_e}^{\infty} [\epsilon_e(z) - \epsilon_{eo}] dz, \quad (47)$$

$$\sigma_\sigma = \int_{-\infty}^{a_\sigma} [\epsilon_\sigma(z) - \epsilon_{\sigma b}] dz + \int_{a_\sigma}^{\infty} [\epsilon_\sigma(z) - \epsilon_{\sigma o}] dz, \quad (48)$$

$$\sigma_\omega = \int_{-\infty}^{a_\omega} [\epsilon_\omega(z) - \epsilon_{\omega b}] dz + \int_{a_\omega}^{\infty} [\epsilon_\omega(z) - \epsilon_{\omega o}] dz, \quad (49)$$

$$\sigma_\rho = \int_{-\infty}^{a_\rho} [\epsilon_\rho(z) - \epsilon_{\rho b}] dz + \int_{a_\rho}^{\infty} [\epsilon_\rho(z) - \epsilon_{\rho o}] dz. \quad (50)$$

The results are shown in Table 3. For sake of comparison we also show the results in the case of ordinary nuclear matter, namely for a system without the presence of electrons. As shown in Eqs. (45)–(50), the contribution of each fermion and meson field to the surface tension strongly depends on the profile and the energy density of the fermion and meson field. As shown in Figs. 1 and 2, comparing to the profiles in the case without the presence of the  $\rho$  meson, the presence of the  $\rho$  meson leads to larger proton and electron densities, and a larger bump of proton density happens. This effect is felt indirectly by neutrons (although much less strong), due to the coupled nature of the system of equations (36)–(39) and (17)–(19). There is no such a bump of the profiles in the case of normal nuclear matter. Comparing the results of the three cases in Table 3, the effect of the bump of proton density on the surface tension is significant. The bump on the profiles decreases the value of the surface tension for fermions and increases the one for bosons. These results provide an evidence of large effect of electromagnetic interaction and electrons on the proton and neutron density profiles, and therefore on the global value of the surface energy of the system.

	$\sigma_n$	$\sigma_p$	$\sigma_e$	$\sigma_\sigma$	$\sigma_\omega$	$\sigma_\rho$
$n p e \sigma \omega$	3.54	−0.36	−1.72	3.16	0.73	
$n p e \sigma \omega \rho$	−27.35	−5.19	−8.34	22.20	19.93	−2.28
$n p \sigma \omega \rho$	19.43	12.23		−16.08	−13.83	−0.04

Table 3: Contribution of each fermion and meson field to the surface tension, in  $\text{MeV fm}^{-2}$ . First row: semi-infinite matter without the presence of the  $\rho$  meson. Second row: semi-infinite matter with the presence of the  $\rho$  meson. Third row: normal nuclear matter (without the presence of electrons). Here the baryon number density in the bulk region is the nuclear saturation density, and the fermion densities and meson fields tend to be zero in the outside region.

#### 2.4. Influence of baryon number density on the surface tension

In order to study the dependence of the surface tension on the baryon number density, we calculate the surface tensions for different  $n_{bb}$  following the similar procedure in Sec. 2.3. The results are shown in Fig. 3. From the results, the total surface tension can be fitted by

$$\sigma_{t,fit} = 1.05 + 2.02 \left( \frac{n_{bb}}{n_{nucl}} \right)^{3.33} (\text{MeV fm}^{-2}), \quad (51)$$

the surface tension for electric field can be fitted by

$$\sigma_{C,fit} = -0.37 + 4.50 \left( \frac{n_{bb}}{n_{nucl}} \right)^2 (\text{MeV fm}^{-2}), \quad (52)$$

and the surface tension for nucleons can be fitted by

$$\sigma_{N,fit} = 0.95 + 6.33 \left( \frac{n_{bb}}{n_{nucl}} \right)^{2.91} (\text{MeV fm}^{-2}). \quad (53)$$

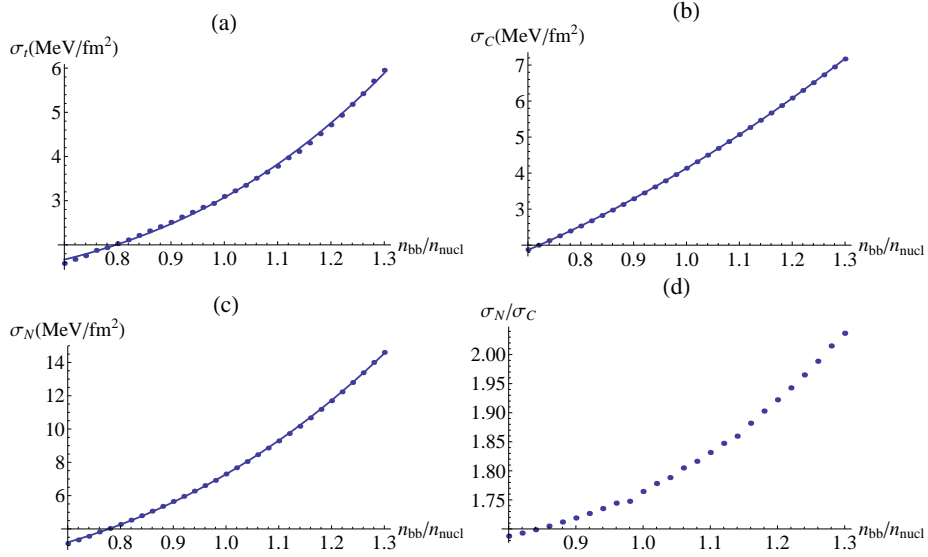


Figure 3: The dependence of the surface tension of semi-infinite matter on the baryon number density in the bulk region. Here the fermion densities and meson fields tend to be zero in the outside region. (a): the total surface tension  $\sigma_t$ , compared with the fit given in Eq. (51). (b): surface tension for electric field  $\sigma_C$ , compared with the fit given in Eq. (52). (c): surface tension for nucleons  $\sigma_N$ , compared with the fit given in Eq. (53). (d): ratio of surface tension for nucleons and the surface tension for electric field  $\sigma_N/\sigma_C$ .

As shown by BBP in [44], the phenomenological surface tension for nucleons within the Thomas-Fermi approximation can be written as

$$\sigma_{sur}^{BBP} = B(W_o - W_i)^{\frac{1}{2}}(n_i - n_o)^{\frac{3}{2}}, \quad (54)$$

where  $B$  is a constant,  $W_o$  and  $W_i$  are the binding energy per nucleon in the outside and inside bulk regions,  $n_o$  and  $n_i$  are the nucleon number density in the outside and inside bulk regions. In the case of this section, we set the fermions densities and meson fields to be zero in the outside region, i.e.  $n_o = W_o = 0$ . Since the fractional concentration of protons in the system we consider here is small, the binding energy per nucleon is [44]

$$W(k, x) = W(k, 0) + f(x) \approx 19.74k^2 - k^3 \frac{40.4 - 1.088k^3}{1 + 2.545k} + f(x), \quad (55)$$

where  $k$  is defined by  $n = 2k^3/(3\pi^2)$ , with  $n$  the nucleon number density, and  $x$  is the fractional concentration of protons. The function  $f(x)$  is a small correction to  $W(k, 0)$  since  $x$  is small in our system. From Eq. (55), one can estimate that the leading term in the binding energy  $W_i$  is the kinetic term, proportional to  $k^2$ , i.e.  $W_i \propto k^2 \propto n_{bb}^{2/3}$ . Thus one can estimate that  $\sigma_{sur}^{BBP} \propto n_{bb}^{11/6}$  in the BBP phenomenological result [44], where the effect of electromagnetic interaction on the profile of fermion density is neglected. This BBP phenomenological result is different from our result in Eq. (53). This is due to the fact that the electromagnetic interaction and the presence of electron change the proton and neutron density profiles.

For  $\sigma_C$ , as shown in Eq. (52) the surface tension for electric field is proportional to the square of the baryon number density. This results can be understood as follows. The Thomas-Fermi equilibrium condition for electrons given by Eq. (17) tell us that the Coulomb potential in the bulk core is proportional to the bulk electron chemical potential, so  $V_b \propto \mu_{eb}$ , and since the electrons are ultra-relativistic at these densities we have  $V_b \propto P_{eb}^F \propto n_{eb}^{1/3}$ . The thickness of the layer is of order  $\Delta r \sim n_{eb}^{-1/3}$  and so the electric field scales as  $E \sim -\Delta V/\Delta r \sim V_b/\Delta r \propto n_{eb}^{2/3}$ . Thus the contribution of the Coulomb energy to the surface tension satisfies  $\sigma_C \propto E^2 \Delta r \propto n_{eb}$  and since in the bulk core we have  $n_{eb} \simeq n_{pb}$  we obtain  $\sigma_C \propto n_{eb} = y n_{bb}$ , where  $y = n_{pb}/n_{bb}$  is the proton fraction in the bulk region. In neutron stars the  $\beta$ -equilibrium between neutrons, protons and electrons leads to a highly nuclear isospin asymmetry ( $y \ll 1$ ), and since the nucleons are approximately non-relativistic and the electrons ultra-relativistic around nuclear saturation density, it can be estimated from Eq. (20) that the proton fraction is proportional to the baryon density, i.e.  $y \propto n_{bb}$ , and therefore we finally obtain our final result  $\sigma_C \propto n_{bb}^2$ .

In Fig. 3 we show also the nuclear to Coulomb surface tension ratio  $\sigma_N/\sigma_C$ . We find that this ratio is larger than unity for all baryon number densities we considered. This would in principle imply that the system is stable with respect to the Bohr-Wheeler condition (34) as we have previously discussed.

It is also worth to mention that the result that  $\sigma_N/\sigma_C > 1$  for every nucleon density in our system can be explained as the result of the penetration of the relativistic electrons into the nucleus (see Refs. [47, 48] for details). This is allowed for a configurations with sufficiently large sizes  $r_0 A^{1/3} > \hbar/(m_e c)$  or mass numbers  $A > \hbar^3/(r_0 m_e c)^3 \sim 10^7$ , where  $r_0 \approx 1.2$  fm. For systems with much larger mass numbers as neutron stars  $A_{NS} \sim 10^{57}$  the penetration of

electrons is such that they nearly neutralize the system and the electric field becomes appreciable only near the core surface [47, 48].

However the transition layer could be unbound if the gravitational binding energy of the shell to the core is smaller than its electrostatic energy. An approximate computation of the stability of the transition layer in the above sense can be found in Ref. [47], where it was shown within Newtonian gravity that the layer is gravitational bound providing the system has a number of baryons  $A \gtrsim 0.004(Z/A)^{1/2}(m_{Pl}/m_N)^3 \sim 10^{55}(Z/A)^{1/2}$  or a mass  $M = m_N A \gtrsim 0.01(Z/A)^{1/2}M_\odot$ , where  $m_N$  and  $m_{Pl} = (\hbar c/G)^{1/2}$  are the nucleon and Planck mass. It is clear that this stability requirement implies a lower limit for our globally neutral neutron stars. It would be interesting to perform a detailed calculation taking into account the effects of general relativity as well as of the magnetic field on the transition surface induced by rotation (see Ref. [52]) and the centrifugal potential acting on the shell. However such calculation is out of the scope of this work and will be presented elsewhere.

### 2.5. Influence of fermion densities in the outside region on the surface tension

As described in Ref. [41] the generalized fermion chemical potentials have to match, at the end of the core-crust transition boundary layer, their corresponding values at the edge of the crust (outside region), i.e. they must satisfy a condition of continuity. This implies a non-zero particle density as matching value. The thickness of the core-crust transition boundary layer as well as the value of the electron density at the edge of the crust  $n_e^{crust}$  depend on the nuclear parameters [41], especially on the nuclear surface tension. So it is important to study the surface structure for different fermion densities in the outside region. The crust is composed by a nuclei lattice in a background of degenerate electrons, whose density at the edge of the crust is denoted here as  $n_e^{crust}$ . There are in addition free neutrons in the crust when the density of the crust  $\rho_{crust}$  is higher than the neutron-drip value  $\rho_{drip} \sim 4.3 \times 10^{11} \text{ g cm}^{-3}$  [44]. So when the density of the crust  $\rho_{crust}$  is smaller than the neutron-drip value, i.e.  $\rho_{crust} < \rho_{drip}$ , we set the proton and neutron densities as zero in the outside region while the electron density must to match the value  $n_e^{crust}$ . In the cases when  $\rho_{crust} > \rho_{drip}$  both neutrons and electrons have to match their corresponding crust values at the end of the core-crust transition layer. As shown by BBP [44] there is no proton-drip at any density of interest in these systems and therefore we keep zero as outside proton density value. In order to set the matching density values for electrons and neutrons we use the relation of the free neutron and electron densities of BBP [44]. At the neutron-drip point the electron Fermi momentum is around  $P_{eo}^F \approx 26 \text{ MeV}$  or  $P_{eo}^F/P_{eb}^F \approx 0.18$ .

Following a similar procedure as in Sec. 2.3, we obtain the fermion density and meson field profiles in this case and calculate its surface tension. The results of the dependence of the surface tension on the outside electron densities and the density of the crust are shown in Fig. 4.

The results of Fig. 4 show that the Bohr-Wheeler condition (34) for the instability is reached at a crust density  $\rho_{crust}^{crit} \sim 1.2 \times 10^{14} \text{ g cm}^{-3}$ , so the system becomes unstable against fission when  $\rho_{crust} > \rho_{crust}^{crit}$ ; imposing a physical upper



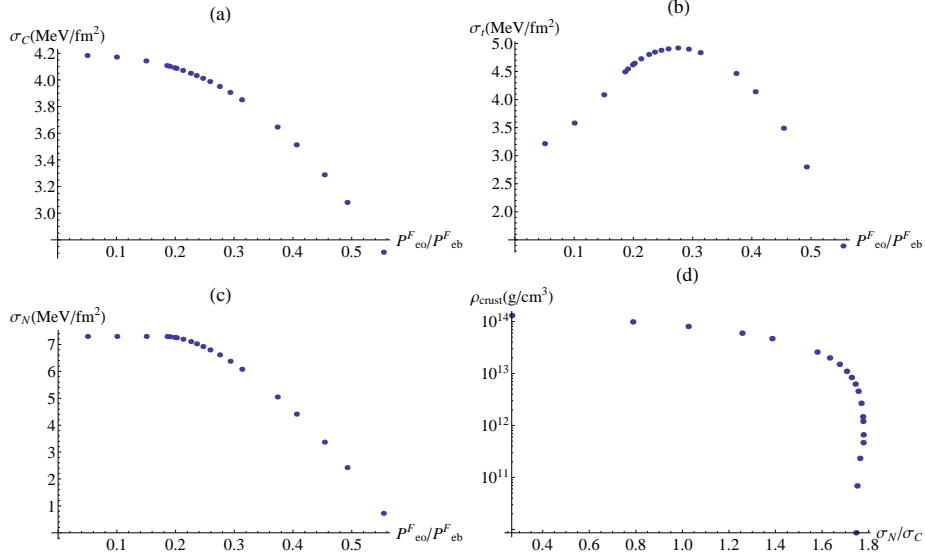


Figure 4: Dependence of the surface tension of semi-infinite matter on the fermion densities in the outside region and the density of the crust. Here the baryon number density of the bulk region is the nuclear saturation density. (a) surface tension for electric field  $\sigma_C$ . (b): the total surface tension  $\sigma_t$ . (c): the surface tension for nucleons  $\sigma_N$ . (d): ratio of the surface tension for nucleons and the surface tension for electric field  $\sigma_N/\sigma_C$ , respect to the density of the crust  $\rho_{crust}$ . The neutron-drip point  $\rho_{drip} \sim 4.3 \times 10^{11} \text{ g cm}^{-3}$  is around  $P_{eo}^F/P_{eb}^F \approx 0.18$ .

limit to the density at the edge of the crust. It becomes interesting to include the binding effect of gravity and any other attractive contribution that strengthen the stability of the system; which will be analyzed elsewhere. It is interesting that this upper limit on the crust density implies a lower limit to the maximum electric field in the core-crust transition region, limiting at the same time to approach a state of quasi-local charge neutrality of the neutron star.

As shown in Fig. 4, the surface tension for electric field decreases as increasing the electron number density in the outside region. The reason is that the increasing electron number density in the outside region [41] causes a decreasing of the thickness of the interface and of the proton and electron density difference, i.e. the surface charge density decreases.

It is shown in Fig. 4 that the dependence of the surface tension for nucleons  $\sigma_N$  on the electron number density in the outside region is weak before the neutron-drip point. The influence of electron density in the outside region on the surface structure of nucleons is small in this case. After the neutron-drip point, the free neutrons in the outside region lower the surface tension significantly, as expected in the BBP phenomenological result [44]. In addition, as shown in Fig. 4, the total surface tension  $\sigma_t$  first increases and then decreases as increasing the fermion densities in the outside region. This is due to the combination of the following two effects. (I) as shown in Table 3, the contribution of electrons to the total surface tension is negative. When increasing the electron density in

the outside region, the effect of electrons on the surface tension becomes weaker. This increases the total surface tension. (II) After the neutron-drip point, the surface tension for nucleons  $\sigma_N$  is lowered significantly by the free neutrons in the outside region.

### 3. Surface properties for neutron star matter with gravitational interaction

#### 3.1. Relativistic equations

Here we add the gravitational interaction to the system we studied above. Taking into account the strong, electromagnetic, weak and gravitational interactions, the total Lagrangian density of the system is given by

$$\mathcal{L}^G = \mathcal{L}_g + \mathcal{L}_f^G + \mathcal{L}_\sigma + \mathcal{L}_\omega + \mathcal{L}_\rho + \mathcal{L}_\gamma + \mathcal{L}_{int}. \quad (56)$$

Here the Lagrangian densities for the gravity is

$$\mathcal{L}_g = -\frac{R}{16\pi G}, \quad (57)$$

where  $G$  is the gravitational constant, and  $R$  is the Ricci scalar. The Lagrangian density for the three fermion species in the gravity field is

$$\mathcal{L}_f^G = \sum_{i=e,N} \bar{\psi}_i (i\gamma^\mu D_\mu - m_i) \psi_i, \quad (58)$$

where  $D_\mu = \partial_\mu + \Gamma_\mu$ , being  $\Gamma_\mu$  the Dirac spin connections. The other parts of the Lagrangian density in Eq. (56) have the same formulations as given in Sec. 2.1.

We introduce the non-rotating spherically symmetric spacetime metric

$$ds^2 = e^{\nu(r)} dt^2 - e^{\lambda(r)} dr^2 - r^2 d\theta^2 - r^2 \sin^2 \theta d\varphi^2, \quad (59)$$

where the  $\nu(r)$  and  $\lambda(r)$  are only functions of the radial coordinate  $r$ .

Within the Thomas-Fermi approximation and mean-field approximation, we can get the full system of general relativistic equations. We are here interested in the core-crust transition layer, which as we have shown happens in a tiny region [41] with a characteristic length scale  $\sim \lambda_e = \hbar/(m_e c) \sim 100$  fm. Correspondingly, the metric functions are essentially constant in this region. Thus in

the core-crust transition layer the system of equations can be written as

$$\frac{d^2 V}{dr^2} + \frac{2}{r} \frac{dV}{dr} = -4\pi e e^{\nu_{core}/2} e^{\lambda_{core}} (n_p - n_e), \quad (60)$$

$$\frac{d^2 \sigma}{dr^2} + \frac{2}{r} \frac{d\sigma}{dr} = e^{\lambda_{core}} [\partial_\sigma U(\sigma) + g_s n_s], \quad (61)$$

$$\frac{d^2 \omega}{dr^2} + \frac{2}{r} \frac{d\omega}{dr} = -e^{\lambda_{core}} (g_\omega J_0^{\omega G} - m_\omega^2 \omega), \quad (62)$$

$$\frac{d^2 \rho}{dr^2} + \frac{2}{r} \frac{d\rho}{dr} = -e^{\lambda_{core}} (g_\rho J_0^{\rho G} - m_\rho^2 \rho), \quad (63)$$

$$E_e^{FG} = e^{\nu_{core}/2} \mu_e - eV = \text{constant}, \quad (64)$$

$$E_p^{FG} = e^{\nu_{core}/2} \mu_p + g_\omega \omega + g_\rho \rho + eV = \text{constant}, \quad (65)$$

$$E_n^{FG} = e^{\nu_{core}/2} \mu_n + g_\omega \omega - g_\rho \rho = \text{constant}, \quad (66)$$

where the notation is the same as in Sec. 2.1. In addition,  $e^{\nu_{core}} \equiv e^{\nu(r_{core})}$  and  $e^{\lambda_{core}} \equiv e^{\lambda(r_{core})}$  are the metric functions evaluated at the core radius  $r_{core}$ . The generalized Fermi energies  $E_e^{FG}$ ,  $E_p^{FG}$ , and  $E_n^{FG}$  (so-called the Klein potentials [38]) are linked by the  $\beta$ -equilibrium of protons, neutrons, and electrons

$$E_n^{FG} = E_p^{FG} + E_e^{FG}. \quad (67)$$

Within the mean-field approximation and Thomas-Fermi approximation, the scalar density  $n_s$  is the same as in the case without gravitational interaction given by Eq. (21) and the non-vanishing components of the currents are

$$J_0^{chG} = e^{\nu_{core}/2} (n_p - n_e), \quad (68)$$

$$J_0^{\omega G} = e^{\nu_{core}/2} (n_n + n_p), \quad (69)$$

$$J_0^{\rho G} = e^{\nu_{core}/2} (n_p - n_n). \quad (70)$$

### 3.2. Surface tension for semi-infinite matter

Since the core-crust transition layer has a characteristic length scale of the order of the electron Compton wavelength, this is very small compared to the radius of neutron stars. So it is a good approximation to use the semi-infinite matter model to construct the surface tension for the system with the electron density  $n_{eb}$  is approximately equal to proton density  $n_{pb}$  in bulk region.

We follow the same procedure described in Sec. 2.2 to construct the surface tension. We assume a surface with small thickness separating two semi-infinite regions (bulk region and outside region). Also we imagine a reference system with a sharp surface at the position  $a_i$  at which the matter and meson fields fall discontinuously from the bulk region to the outside region. Following the definition of fermion number in curved space-time Eq. (59) (see e.g. [53]), the  $i$ -specie fermion number  $N_i$  is given by

$$N_i = 4\pi \int e^{\lambda/2} r^2 n_i(r) dr. \quad (71)$$

Since the metric functions are constant in the surface region we consider as described in Sec. 3.1, and the size of the surface region is very small compared to the radius of neutron stars, we can treat  $e^{\lambda/2}r^2$  as a constant in the integral, the location of the reference surfaces of fermions and meson fields have the similar expressions in Eq. (28) and Eq. (29)

$$\int_{-\infty}^{a_i} dr[n_i(r) - n_{ib}] + \int_{a_i}^{\infty} dr[n_i(r) - n_{io}] = 0; \quad i = n, p, e, \quad (72)$$

$$\int_{-\infty}^{a_i} dr[F_i(r) - F_{ib}] + \int_{a_i}^{\infty} dr[F_i(r) - F_{io}] = 0; \quad i = \sigma, \omega, \rho, \quad (73)$$

where  $n_i(r)$  is the number density of the  $i$ -specie fermion, and  $F_i(r)$  is the time component of the  $i$ -specie meson field.

The energy associated to the density  $\varepsilon(r) = T_0^0$ , where  $T_\beta^\alpha$  is the energy-momentum tensor of the system, can be calculated in the spherically symmetric metric by (see e.g. [53])

$$E = 4\pi \int e^{(\nu+\lambda)/2} r^2 \varepsilon(r) dr. \quad (74)$$

So we can calculate the total surface tension by

$$\begin{aligned} \sigma_t^G = & \sum_{i=n,p,e,\sigma,\omega,\rho} e^{(\nu_{core}+\lambda_{core})/2} \left\{ \int_{-\infty}^{a_i} [\epsilon_i^G(r) - \epsilon_{ib}^G] dr + \int_{a_i}^{\infty} [\epsilon_i^G(r) - \epsilon_{io}^G] dr \right\} \\ & + e^{(\nu_{core}+\lambda_{core})/2} \int_{-\infty}^{\infty} \epsilon_E^G(r) dr, \end{aligned} \quad (75)$$

where  $\epsilon_i^G(r)$  is the energy density of the  $i$ -specie fermion or meson field,  $\epsilon_{ib}^G$  is the energy density of the  $i$ -specie fermion or meson field in the bulk region,  $\epsilon_{io}^G$  is the energy density of the  $i$ -specie fermion or meson field in the outside region, and  $\epsilon_E(r)^G$  is the energy density of the electric field.

For later discussions, we define the surface tension for nucleons as

$$\sigma_N^G = \sum_{i=n,p,\sigma,\omega,\rho} e^{(\nu_{core}+\lambda_{core})/2} \left\{ \int_{-\infty}^{a_i} [\epsilon_i^G(r) - \epsilon_{ib}^G] dr + \int_{a_i}^{\infty} [\epsilon_i^G(r) - \epsilon_{io}^G] dr \right\}, \quad (76)$$

and the surface tension for electric field as

$$\sigma_C^G = e^{(\nu_{core}+\lambda_{core})/2} \int_{-\infty}^{\infty} \epsilon_E^G(r) dr. \quad (77)$$

The energy density of the  $i$ -specie fermion  $\epsilon_i^G(r)$  has the same formulation as

Eq. (40), and the energy densities of the meson fields are (see e.g. [53])

$$\epsilon_\sigma^G(r) = \frac{1}{2}e^{-\lambda_{core}}\left(\frac{d\sigma}{dr}\right)^2 + U(\sigma), \quad (78)$$

$$\epsilon_\omega^G(r) = \frac{1}{2}e^{-(\lambda_{core}+\nu_{core})}\left(\frac{d\omega}{dr}\right)^2 + \frac{1}{2}e^{-\nu_{core}}m_\omega^2\omega^2, \quad (79)$$

$$\epsilon_\rho^G(r) = \frac{1}{2}e^{-(\lambda_{core}+\nu_{core})}\left(\frac{d\rho}{dr}\right)^2 + \frac{1}{2}e^{-\nu_{core}}m_\rho^2\rho^2, \quad (80)$$

$$\epsilon_E^G(r) = e^{-(\lambda_{core}+\nu_{core})}\frac{1}{8\pi}\left(\frac{dV}{dr}\right)^2. \quad (81)$$

As described in Ref. [41], fields vary slowly in the core of neutron stars, so it is a good approximation to treat the bulk region as the uniform matter. For the uniform matter, the equations (61)-(63) reduce to

$$0 = \partial_\sigma U(\sigma) + g_s n_s, \quad (82)$$

$$0 = g_\omega J_0^{\omega G} - m_\omega^2 \omega, \quad (83)$$

$$0 = g_\rho J_0^{\rho G} - m_\rho^2 \rho. \quad (84)$$

Following the similar procedure in Sec. 2.3, we solve the Eqs. (60)-(66) to obtain the fermion density and meson field profiles. We assume the baryon number density in the bulk region to be the nuclear saturation density,  $n_{bb} = n_{nb} + n_{pb} = n_{nucl} = 0.16 \text{ fm}^{-3}$ . We have again assumed  $n_{pb} \simeq n_{eb}$  in the bulk (core) region, and we set the fermion densities and meson fields to be zero in the outside region for sake of comparison with the previous results of Fig. 1. At the core-radius (in this case the surface) of the neutron star, the metric functions have to match the Schwarzschild solution due to the global neutrality condition, so at the border of the star we have

$$e^{\nu_{core}} = e^{-\lambda_{core}} = 1 - \frac{2GM(r_{core})}{r_{core}}, \quad (85)$$

with  $M(r_{core})$  the total mass of the star. The results of the solution are shown in Fig. 5 for the case  $e^{\lambda_{core}} = e^{-\nu_{core}} = 1.5$ .

In curved spacetime, the electric field is given by (see e.g. [41])

$$|E| = e^{-(\lambda_{core}+\nu_{core})/2}\frac{dV}{dr}. \quad (86)$$

Comparing to the results shown in Fig. 1, the fermion density and meson field profiles are similar to their counterparts in the case without the gravitational field. In Fig. 5 we see a larger proton density, a smaller neutron density, and a smaller size of the core-crust transition layer leading to a larger maximum of the electric field, comparing to Fig. 1.

Using the definitions in Eqs. (75)-(77), we obtain the surface tensions for the transition layer of this system. Fig. 6 shows the results of the dependence

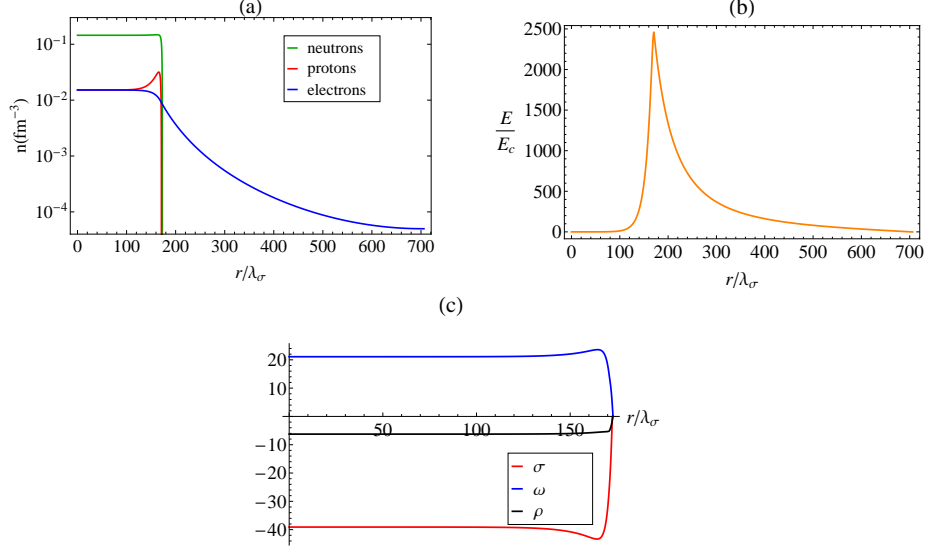


Figure 5: (a): fermion density profiles in units of  $\text{fm}^{-3}$ . (b): electric field in units of the critical field  $E_c$ . (c): meson fields  $\sigma$ ,  $\omega$ , and  $\rho$  in the unit of MeV. Here we set  $e^{\lambda_{core}} = e^{-\nu_{core}} = 1.5$ , the baryon number density in the bulk region is the nuclear saturation density, and the fermion densities and meson fields tend to be zero in the outside region.

of the surface tension on the value of metric  $e^{\lambda_{core}}$ . As shown in Fig. 6, the total surface tension and the surface tension for nucleons increase as increasing the value of the metric  $e^{\lambda_{core}}$ . As described in Sec. 2.2, the surface tension mainly depends on the profiles of the fermion and meson densities and energy densities. There are two effects which influence on the characters of the total surface tension and the surface tension for nucleons. First, as we have seen the presence of gravitational field changes the fermion density and meson field profiles. Second, the difference between the proton density and the neutron density becomes smaller when the value of the metric  $e^{\lambda_{core}}$  increases; lowering the isospin asymmetry of the system. The combination of these two effects leads to the characters of the total surface tension and the surface tension for nucleons shown in Fig. 6. In addition, as shown in Fig. 6, the change of the value of the surface tension for electric field when increasing the value of  $e^{\lambda_{core}}$  is small. That is due to the balance of the following two effects: (I) the electric field in the surface region becomes larger (see Fig. 5); (II) the thickness of the surface becomes smaller, and then the Coulomb energy distributes in a smaller region. It can be also checked from Fig. 5 how in the limit  $e^{\lambda_{core}} \rightarrow 1$  all quantities tend to the values found in Sec. 2.3 in the flat case.

#### 4. Surface tension for the system with small electron density

Now we turn to consider a system with the electron density in the bulk region smaller than the proton one, i.e.  $n_{eb} < n_{bp}$ , to study the effects of electrons

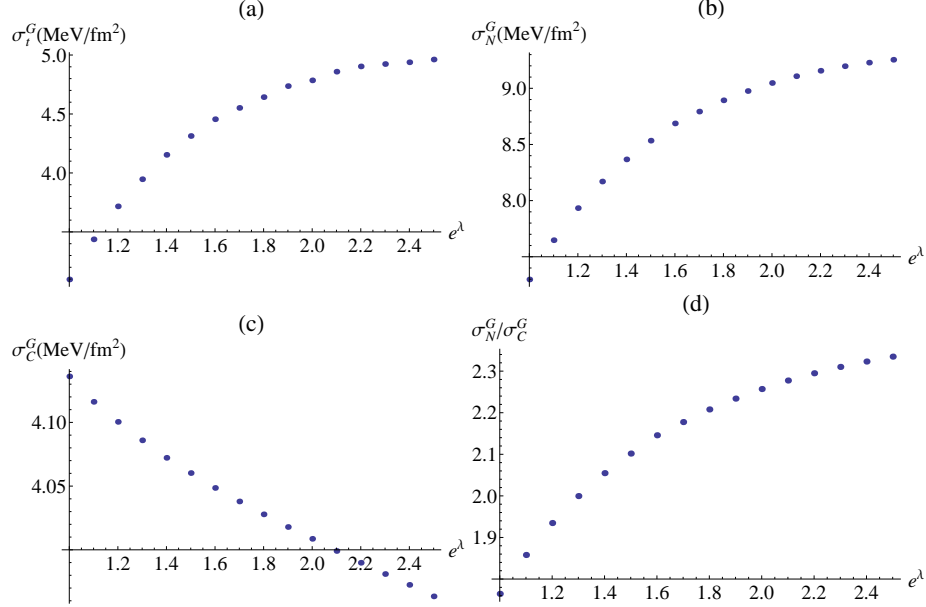


Figure 6: The dependence of the surface tension of semi-infinite matter on the value of metric  $e^{\lambda_{core}}$ . (a): the total surface tension  $\sigma_t^G$ . (b): surface tension for nucleons  $\sigma_N^G$ . (c): surface tension for electric field  $\sigma_C^G$ . (d): ratio of surface tension for nucleons and the surface tension for electric field  $\sigma_N^G/\sigma_C^G$ . Here the baryon number density in the bulk region is the nuclear saturation density, and the fermion densities and meson fields tend to be zero in the outside region.

on the surface structure and surface tension. In this section we did not take into account the gravitational field. In order to construct the surface tension, we consider this system as a superheavy nucleus whose nucleon number is so large that electrons can penetrate inside the nucleus. We adopt this superheavy nucleus as a spherical droplet, so we have spherical symmetry in this system. We assume a spherical surface (the size of the system we consider here is larger than ordinary nuclei, so the curvature energy here is small compared to the surface energy) with small thickness separating one finite region (inside the nuclear region) and one semi-infinite region (outside region). The number density of the  $i$ -specie fermion  $n_i(r)$  approaches the density of the  $i$ -specie fermion  $n_{ib}$  in the origin as the position  $r \rightarrow 0$ , and approaches the density in the outside region of the  $i$ -specie fermion  $n_{io}$  as the  $r \rightarrow +\infty$ . To construct the surface tension, as in the case of the semi-infinite matter model, we imagine a reference system with a sharp surface at radius  $r_i$  at which the matter and meson fields fall discontinuously from the bulk region to the outside region. Following the similar method of BBP [44], the location of the reference surface for the  $i$ -specie fermion is defined by the condition that the reference system has the same

number of  $i$ -specie fermion as the original system

$$4\pi \int_0^{r_i} r^2 dr [n_i(r) - n_{ib}] + 4\pi \int_{r_i}^{\infty} r^2 dr [n_i(r) - n_{io}] = 0; \quad i = n, p, e. \quad (87)$$

Similar to definition of reference surface for fermions, the location of the reference surfaces for meson fields are defined by

$$4\pi \int_0^{r_i} r^2 dr [F_i(r) - F_{ib}] + 4\pi \int_{r_i}^{\infty} r^2 dr [F_i(r) - F_{io}] = 0; \quad i = \sigma, \omega, \rho, \quad (88)$$

where  $F_i(r)$  is the time component of the  $i$ -specie meson field,  $F_{ib}$  is the time component of the  $i$ -specie meson field in the inside region, and  $F_{io}$  is the time component of the  $i$ -specie meson field in the outside region.

Similar to the way of BBP [44], the surface energy can be computed as the total energy subtracting off the bulk energy,

$$E_{sur} = \sum_{i=n,p,\sigma,\omega,\rho} \left\{ 4\pi \int_0^{r_i} r^2 [\epsilon_i(r) - \epsilon_{ib}] dr + 4\pi \int_{r_i}^{\infty} r^2 [\epsilon_i(r) - \epsilon_{io}] dr \right\}, \quad (89)$$

and the Coulomb energy is

$$E_{coul} = 4\pi \int_0^{\infty} r^2 \epsilon_E(r) dr, \quad (90)$$

where  $\epsilon_i(r)$  is the energy density of the  $i$ -specie fermion or meson field,  $\epsilon_{ib}$  is the energy density of the  $i$ -specie fermion or meson field in the center of the system,  $\epsilon_{io}$  is the energy density of the  $i$ -specie fermion or meson field in the outside region, and  $\epsilon_E(r)$  is the energy density of the electric field. The surface tension for nucleons is given as the surface energy per unit area,

$$\sigma_{Ns} = \frac{E_{sur}}{4\pi r_n^2}, \quad (91)$$

and similarly we obtain the Coulomb energy per unit area

$$\sigma_{Cs} = \frac{E_{coul}}{4\pi r_n^2}, \quad (92)$$

where  $r_n$  is the reference radius of neutrons defined by Eq. (87). Since the neutron number is much larger than the proton number in the system, so it is reasonable to set the radius of neutrons to be the radius of nucleus to estimate the surface tension; this is consistent with the existence of the neutrons halo or neutron skin effect.



For this spherical system, the equations (13)-(16) become

$$\frac{d^2 V}{dr^2} + \frac{2}{r} \frac{dV}{dr} = -4\pi e(n_p - n_e), \quad (93)$$

$$\frac{d^2 \sigma}{dr^2} + \frac{2}{r} \frac{d\sigma}{dr} = \partial_\sigma U(\sigma) + g_s n_s, \quad (94)$$

$$\frac{d^2 \omega}{dr^2} + \frac{2}{r} \frac{d\omega}{dr} = -(g_\omega J_0^\omega - m_\omega^2 \omega), \quad (95)$$

$$\frac{d^2 \rho}{dr^2} + \frac{2}{r} \frac{d\rho}{dr} = -(g_\rho J_0^\rho - m_\rho^2 \rho). \quad (96)$$

The energy density of the i-specie fermion  $\epsilon_i(r)$  has the same formulation as Eq. (40), and the energy densities of the meson fields in this spherical system are

$$\epsilon_\sigma(r) = \frac{1}{2} \left( \frac{d\sigma}{dr} \right)^2 + U(\sigma), \quad (97)$$

$$\epsilon_\omega(r) = \frac{1}{2} \left( \frac{d\omega}{dr} \right)^2 + \frac{1}{2} m_\omega^2 \omega^2, \quad (98)$$

$$\epsilon_\rho(r) = \frac{1}{2} \left( \frac{d\rho}{dr} \right)^2 + \frac{1}{2} m_\rho^2 \rho^2, \quad (99)$$

$$\epsilon_E(r) = \frac{1}{8\pi} \left( \frac{dV}{dr} \right)^2. \quad (100)$$

Following the similar procedure in Sec. 2.3, we solve the equations (93)-(96) and (17)-(19) to obtain the fermion density and meson field profiles. We assume the baryon number density in the region near the center to be the nuclear saturation density,  $n_{bb} = n_{nb} + n_{pb} = n_{nucl} = 0.16 \text{ fm}^{-3}$ , and we set a small electron density  $n_{eb} = y_e n_{pb}$  in the region near the center with electron fraction  $y_e < 1$ . We set the fermion densities and meson fields to be zero in the outside region. The results of the solution are shown in Fig. 7 for the case  $P_e^F = 0.95 P_p^F$  in the region near the center of the system, and in Fig. 8 for the case  $P_e^F = 0.5 P_p^F$  in the region near the center of the system.

As shown in Fig. 7, when the difference between the electron and proton density in the region near the center of the system ( $n_{pb} - n_{eb}$ ) is small, the fermion density and meson field profiles are similar to their counterparts in the case of semi-infinite matter (electron density nearly equal to the proton density in the bulk region  $n_{eb} \simeq n_{pb}$ ). Comparing to the results in the case of semi-infinite matter in Fig. 1, the bump of the proton profile is larger in this case, as expected from the fact that the internal electric field is less screened in this case than when  $n_{eb} \simeq n_{pb}$ . We can also see how the fermion and meson field profiles change for increasing charge separations  $n_{pb} - n_{eb}$ .

Using the definitions in Eqs. (91) and (92), we obtain the surface tensions for the transition layer of this system. The results of the dependence of the surface tension on the ratio of the electron Fermi momentum and the proton Fermi

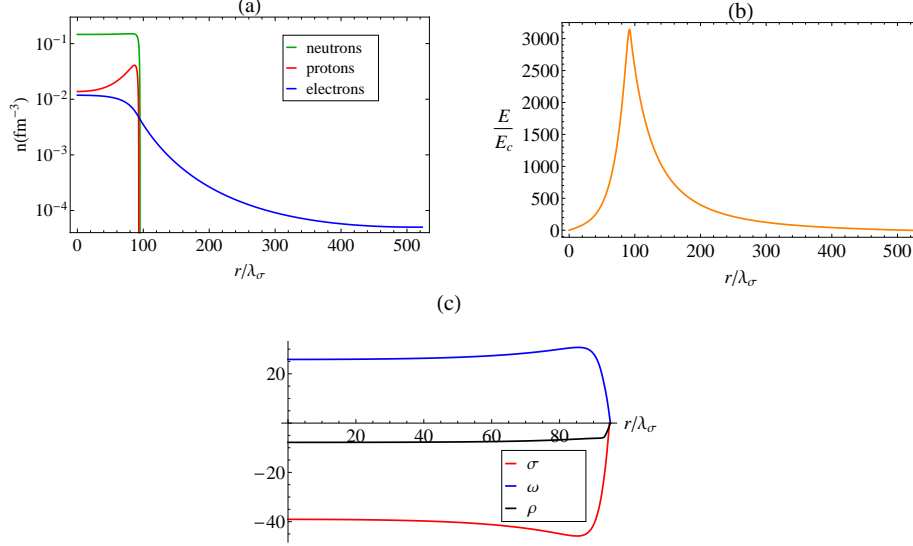


Figure 7: (a): fermion density profiles in units of  $\text{fm}^{-3}$ . (b): electric field in units of the critical field  $E_c$ . (c): meson fields  $\sigma$ ,  $\omega$ , and  $\rho$  in the unit of MeV. Here we set  $P_e^F = 0.95P_p^F$  in the region near the center of the system, the baryon number density in the region near the center is the nuclear saturation density, and the fermion densities and meson fields tend to be zero in the outside region.

momentum in the region near the center of the system ( $P_{eb}^F/P_{pb}^F$ ) are shown in Fig. 9. From the results, the system is stable with respect to the Bohr-Wheeler condition Eq. (34) of the stability, in all ratios  $P_{eb}^F/P_{pb}^F$  we considered. As shown in Fig. 9, the surface tension for nucleons first increases and then decreases when the difference between the electron and proton density increases, and the surface tension tends to the phenomenological result ( $\sim 1 \text{ MeV fm}^{-2}$ ) in nuclear physics without the presence of electrons in the inside bulk region [44]. There are two effects which influence on the surface tension for nucleons: (I) for  $n_{eb} < n_{pb}$  the bump of the proton profile around the nuclear surface enhances as shown in Figs. 7–8, and (II) the higher the difference  $n_{pb} - n_{eb}$  the lower the nuclear asymmetry. As a consequence, the total energy of the system decreases. The combination of these two effects leads to the results of the surface tension for nucleons shown in Fig. 9.

## 5. Summary

Taking into account strong, weak, electromagnetic, and gravitational interactions, and fulfilling the global charge neutrality of the system, a transition layer will happen between the core and crust of neutron stars [41]. This is different from the results from traditional TOV equations imposing local charge neutrality. This core-crust transition layer happens at the saturation density of nuclear matter. In this article, using RMFT together with the Thomas-Fermi

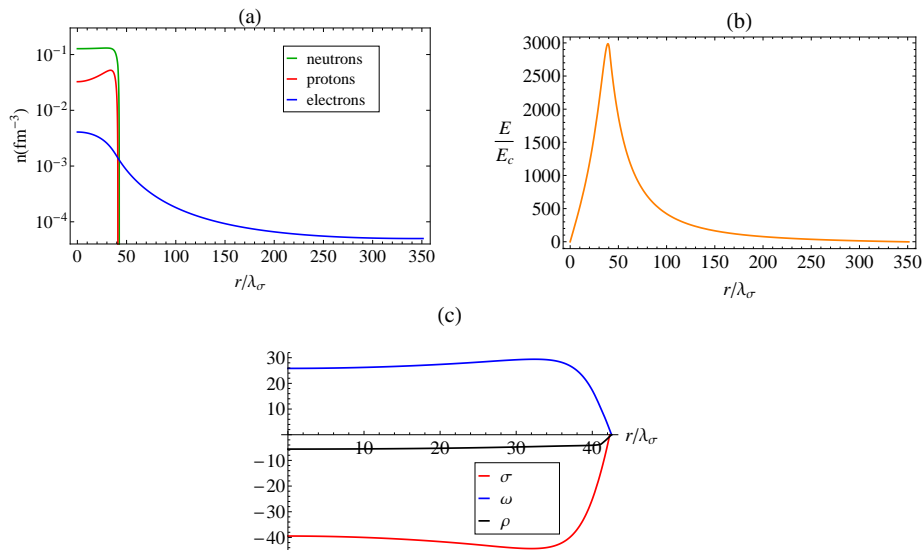


Figure 8: (a): fermion density profiles in units of  $\text{fm}^{-3}$ . (b): electric field in units of the critical field  $E_c$ . (c): meson fields  $\sigma$ ,  $\omega$ , and  $\rho$  in the unit of MeV. Here we set  $P_e^F = 0.5P_p^F$  in the region near the center of the system, the baryon number density in the region near the center is the nuclear saturation density, and the fermions densities and meson fields tend to be zero in the outside region.

approximation, we give a detailed description of the structure of this transition layer. We computed the surface tension and Coulomb energy of the transition shell and analyze the role of each fermion component and meson fields in the determination of the properties of this core-crust transition layer.

Following the method of Baym, Bethe and Pethick in Ref. [44], we applied the semi-infinite matter model to construct the surface tension for the transition layer of this system with the electron density is approximately equal to the proton density in the bulk region. The results show that, in the surface region, a proton bump appears due to Coulomb repulsion. The neutron skin effect and electron screening effect are described in detail. We calculated the surface tension and the Coulomb energy for the transition layer of this system for different baryon number densities near the nuclear saturation density. The results show that the total surface tension as well as surface tension for electric field and the surface tension for nucleons are proportional to some power-law function of the baryon number density in the bulk region; see Eqs. (51), (53) and (52). The difference between the surface energy of this neutron star matter and the phenomenological results [44] in nuclear physics has been analyzed. We also studied the surface structure for different fermion densities in the outside region, namely for different densities of the neutron star crust.

We presented this analysis both in flat and curved spacetime. In the latter case we treated the system in the background of non-rotating spherically symmetric case as in Ref. [41]. Since the length scale (the order of the elec-

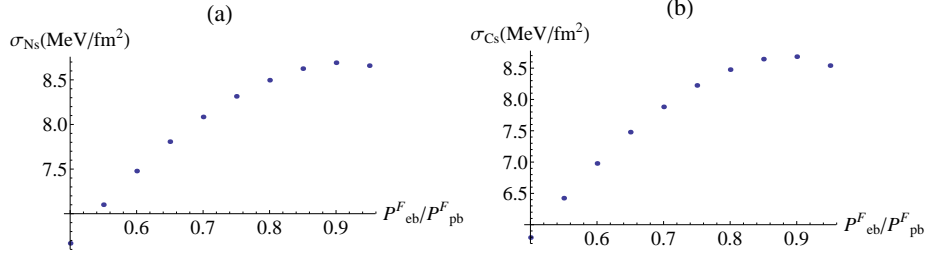


Figure 9: The dependence of the surface tension on the ratio  $P_{eb}^F/P_{pb}^F$ .  $P_{eb}^F$  is the Fermi momentum of electrons in the region near the center of the system, and  $P_{pb}^F$  is the Fermi momentum of protons in the region near the center of the system. The baryon number density in the region near the center is the nuclear saturation density, and the fermion densities and meson fields tend to be zero in the outside region. (a): surface tension for nucleons,  $\sigma_{Ns}$ . (b): Coulomb energy per unit area,  $\sigma_{Cs}$ .

tron Compton wavelength) of the core-crust transition layer is much smaller than the radius of neutron stars, we used the semi-infinite matter model as an approximation to construct the surface tension for the transition layer of this system with the electron density is approximately equal to the proton density in the bulk region. The results show that the fermion density and meson field profiles are similar to the case without the presence of gravitational field, although some quantitative differences appear. We show that the total surface tension and the surface tension for nucleons increase as increasing the value of the metric function  $e^{\lambda_{core}}$ .

We then calculated the surface tension and the Coulomb energy for the transition layer of the system with the electron density is smaller than the proton density in the bulk region using the spherical droplet model. We show how the surface tension and the electrostatic energy per unit area are drastically affected by the increasing proton repulsion and decreasing nuclear asymmetry with a decreasing electron to proton density ratio (see Figs. 7, 8 and 9).

We studied the instability against Bohr-Wheeler surface deformation for all the systems. We find that the instability sets in at a critical density of the crust  $\rho_{crust}^{crit} \sim 1.2 \times 10^{14} \text{ g cm}^{-3}$ . This implies a lower limit to the maximum electric field of the core-crust transition region and makes inaccessible a state of quasi-local charge neutrality for the neutron star, which will in principle be reached when the limit  $\rho_{crust} = \rho_{core} \approx \rho_{nuc}$ , is approached.

The results of this work open the way to more general studies relevant for the analysis of the stability of neutron stars and the core-crust transition surface. Some of the effects that need to be addressed for the stability of the shell include gravitational binding, centrifugal repulsion, magnetic field induced by rotating electric field and hence magnetic dipole-dipole interactions. It would be interesting to perform a similar analysis for the case of strange stars both bare and in presence of outer crust.

As pointed out in Ref. [54], the frequencies of shear oscillations due to the hadron-quark mixed phase in neutron stars depend strongly on the surface ten-

sion of the hadron-quark interface. It would be interesting to perform a analysis for the dependence of the surface waves on the surface tension of the core-crust transition surface.

### Acknowledgement

Yuan-Bin Wu is supported by the Erasmus Mundus Joint Doctorate Program by Grant Number 2011-1640 from the EACEA of the European Commission.

### References

- [1] H. P. Duerr, Phys. Rev. 103 (1956) 469.
- [2] L. D. Miller and A. E. S. Green, Phys. Rev. C 5 (1972) 241.
- [3] J. D. Walecka, Ann. Phys. 83 (1974) 491.
- [4] J. Boguta and J. Rafelski, Phys. Lett. B 71 (1977) 22.
- [5] J. Boguta and A. R. Bodmer, Nucl. Phys. A 292 (1977) 413.
- [6] T. D. Lee and G. C. Wick, Phys. Rev. D 9 (1974) 2291.
- [7] T. D. Lee, Rev. Mod. Phys. 47 (1975) 267.
- [8] T. D. Lee, M. Margulies, Phys. Rev. D 11 (1975) 1591.
- [9] J. Boguta and H. Stöcker, Phys. Lett. B 120 (1983) 289.
- [10] J. Boguta and S. A. Moszkowski, Nucl. Phys. A 403 (1983) 445.
- [11] J. Boguta, Nucl. Phys. A 501 (1989) 637.
- [12] B. D. Serot, Rept. Prog. Phys. 55 (1992) 1855.
- [13] P. Ring, Prog. Part. Nucl. Phys. 37 (1996) 193.
- [14] M. Bender, P.-H. Heenen, and P.-G. Reinhard, Rev. Mod. Phys. 75 (2003) 121.
- [15] T. Maruyama, T. Tatsumi, D. N. Voskresensky, T. Tanigawa, and S. Chiba, Phys. Rev. C 72 (2005) 015802.
- [16] S. S. Avancini, D. P. Menezes, M. D. Alloy, J. R. Marinelli, M. M. W. de Moraes, and C. Providência, Phys. Rev C 78 (2008) 015802.
- [17] M. Okamoto, T. Maruyama, K. Yabana, and T. Tatsumi, Phys. Lett. B 713 (2012) 284.
- [18] F. Grill, C. Providência, and S. S. Avancini, Phys. Rev. C 85 (2012) 055808.
- [19] R. J. Furnstahl, B. D. Serot, and H. B. Tang, Nucl. Phys. A 598 (1996) 539.

- [20] R. J. Furnstahl, B. D. Serot, and H. B. Tang, Nucl. Phys. A 615 (1997) 441; A640 (1998) 505.
- [21] B. D. Serot and J. D. Walecka, Int. J. Mod. Phys. E 6 (1997) 515.
- [22] M. Brack, C. Guet, and H.-B. Håkansson, Phys. Rep. 123 (1985) 275.
- [23] M. M. Sharma, S. A. Moszkowski, and P. Ring, Phys. Rev. C 44 (1991) 2493.
- [24] D. Von-Eiff, J. M. Pearson, W. Stocker, and M. K. Weigel, Phys. Lett. B 324 (1994) 279.
- [25] D. Von-Eiff, W. Stocker, and M. K. Weigel, Phys. Rev. C 50 (1994) 1436.
- [26] D. Von-Eiff, H. Freyer, W. Stocker, and M. K. Weigel, Phys. Lett. B 344 (1995) 11.
- [27] M. Centelles, M. D. Estal, and X. Viñas, Nucl. Phys. A 635 (1998) 193.
- [28] M. D. Estal, M. Centelles, and X. Viñas, Nucl. Phys. A 650 (1999) 443.
- [29] S. K. Patra, M. Centelles, X. Viñas, and M. D. Estal, Phys. Rev. C 65 (2002) 044304.
- [30] P. Danielewicz and J. Lee, Nucl. Phys. A 818 (2009) 36.
- [31] N. K. Glendenning, Phys. Rev. D 46 (1992) 1274.
- [32] N. K. Glendenning, Phys. Rep. 342 (2001) 393.
- [33] N. K. Glendenning and J. Schaffner-Bielich, Phys. Rev. C 60 (1999) 025803.
- [34] M. B. Christiansen, N. K. Glendenning, and J. Schaffner-Bielich, Phys. Rev. C 62 (2000) 025804.
- [35] M. Alford, K. Rajagopal, S. Reddy, and F. Wilczek, Phys. Rev. D 64 (2001) 074017.
- [36] D. G. Ravenhall, C. J. Pethick, and J. R. Wilson, Phys. Rev. Lett. 50 (1983) 2066.
- [37] M. Rotondo, J. A. Rueda, R. Ruffini, and S.-S. Xue, Phys. Lett. B 701 (2011) 667.
- [38] J. A. Rueda, R. Ruffini, and S.-S. Xue, Nucl. Phys. A 872 (2011) 286.
- [39] R. C. Tolman, Phys. Rev. 55 (1939) 364.
- [40] J. R. Oppenheimer and G. Volkoff, Phys. Rev. 55 (1939) 374.
- [41] R. Belvedere, D. Pugliese, J. A. Rueda, R. Ruffini, and S.-S. Xue, Nucl. Phys. A 883 (2012) 1.

- [42] P. Haensel, A. Y. Potekhin, and D. G. Yakovlev, *Neutron Stars 1: Equation of State and Structure*, Springer-Verlag, New York, 2007.
- [43] N. Bohr and J. A. Wheeler, *Phys. Rev.* 56 (1939) 426.
- [44] G. Baym, H. A. Bethe, and C. J. Pethick, *Nucl. Phys. A* 175 (1971) 225.
- [45] J. Boguta, *Phys. Lett. B* 106 (1981) 255.
- [46] B. Cameron, *Eur. J. Phys.* 30 (2009) 763.
- [47] M. Rotondo, R. Ruffini, S.-S. Xue, and V. Popov, *Int. J. Mod. Phys. D* 20 (2011) 1995.
- [48] M. Rotondo, J. A. Rueda, R. Ruffini, and S.-S. Xue, *Phys. Rev. C* 83 (2011) 045805.
- [49] P.-G. De Gennes, F. Brochard-Wyart, and D. Quéré, *Capillary and Wetting Phenomena Drops, Bubbles, Pearls, Waves*, Springer, New York, 2003.
- [50] G. A. Lalazissis, J. König, and P. Ring, *Phys. Rev. C* 55 (1997) 540.
- [51] A. Tamii, *et al.*, *Phys. Rev. Lett.* 107 (2011) 062502.
- [52] K. Boshkayev, M. Rotondo, and R. Ruffini, *Int. J. Mod. Phys. Conf. S.* bf 12 (2012) 58.
- [53] T. D. Lee and Y. Pang, *Phys. Rev. D* 35 (1987) 3678.
- [54] H. Sotani, T. Maruyama, and T. Tatsumi, *Nucl. Phys. A* 906 (2013) 37.